PERGAMON

Deep-Sea Research II 50 (2003) 299–319

DEEP-SEA RESEARCH
PART II

www.elsevier.com/locate/dsr2

Modeling the initial, fast Sea-Surface Height decay of Agulhas ring "Astrid"

S.S. Drijfhout[a,*], C.A. Katsman[b], L. de Steur[b], P.C.F. van der Vaart[b], P.J. van Leeuwen[b], C. Veth[c]

[a] *Royal Netherlands Meteorological Institute (KNMI), P.O. Box 201, 3730 AE, De Bilt, Netherlands*
[b] *Institute for Marine and Atmospheric Research, Utrecht University, P.O. Box 80005, 3508 TA Utrecht, Netherlands*
[c] *Netherlands Institute for Sea Research, P.O Box 59, 1790 AB Den Burg, Texel, Netherlands*

Received 17 September 2001; received in revised form 7 May 2002; accepted 30 July 2002

Abstract

The early Sea-Surface Height (SSH) decay of an Agulhas ring is studied using a circular symmetric, equivalent barotropic idealization of ring Astrid, which was measured during the first MARE-cruise. Observations indicate that the SSH of Agulhas rings most rapidly decays just after shedding. It is found that the observed initial fast decay of ring Astrid can be recovered by a numerical model and that a mixed baroclinic/barotropic instability accounts for most of the observed decay of SSH.

In addition, a series of numerical experiments is presented in which the effects on the decay of ring strength, barotropic component, diameter, radial profile, β, and cooling were investigated. In all cases discussed, rings are linearly unstable to an $m = 2$ mode. The evolution of the first 10 days is well predicted by a linear stability analysis. Further growth of the $m = 2$ mode leads in most cases to split-up of the ring. The SSH decay of the rings is associated with a conversion from available potential energy of the parent ring to kinetic energy of nearly barotropic higher modes. Most of the energy release is associated with the $m = 2$ mode. Also, the parent ring features an energy conversion from its barotropic to its baroclinic components.

A strong barotropic component associated with a corotating ring is essential for SSH decay to occur. Counterrotating rings may feature SSH increase by energy conversion from the baroclinic to the barotropic component. For corotating rings SSH decay becomes weaker when the instability develops less vigorous. The simulation of ring Astrid shows that tracer loss from the core scales well with the decay of SSH. In the thermocline the associated mixing of fluid occurs preferably at the extremes of the elongating ring. At the deepest levels mixing is associated with dispersion through Rossby-wave radiation.

1. Introduction

In the upper branch of the thermohaline circulation (THC) a critical link is formed by the heat and salt exchanges between the Indian and Atlantic oceans around South Africa (e.g.,

*Corresponding author. Tel:. +31-30-2206395; fax: +31-30-2202570.
E-mail address: drijfhou@knmi.nl (S.S. Drijfhout).

0967-0645/02/$ - see front matter © 2002 Elsevier Science Ltd. All rights reserved.
PII: S0967-0645(02)00386-7

Gordon et al., 1992, Schmitz 1995; De Ruijter et al., 1999). This interocean exchange varies strongly on seasonal and interannual time scales. Its variability is directly linked to the intermittent shedding of large Agulhas rings at the Agulhas Retroflection that carry their anomalous Indian Ocean properties into the South Atlantic (Van Ballegooyen et al., 1994, Goñi et al., 1997). Transport of mainly South Indian Central Water (SICW) establishes the so-called warm-water route of the THC, Gordon (1986). How SICW is brought into the THC is not well understood at present. Available data suggest that the warm-water route follows the Benguela Current and South Equatorial Current from southwest Africa to the coast of Brazil (Peterson and Stramma, 1991, Garzoli et al., 1996), where the water is transported across the equator by the North Brazil (Under)Current. Agulhas rings, however, follow a different route. From satellite images a Ring Corridor has been established that crosses the Benguela Current and its source waters in the southeast Atlantic (Garzoli et al., 1996; Goñi et al., 1997).

To contribute to the upper branch of the THC, Agulhas rings have to yield part of their water mass properties in the southeast Atlantic when they cross the Benguela Current and its source waters. The remainder of the rings then recirculates in the wind driven "super"-gyre that connects the subtropical gyres of the South Indian and South Atlantic Oceans (De Ruijter et al., 1999). From an Agulhas Ring Census (Van Ballegooyen et al., 1994; Duncombe Rae et al., 1996), it is known that Agulhas rings quickly loose mass and energy after being spawned. Also from satellite altimetry Schouten et al. (2000) observed that the SSH of Agulhas rings most rapidly decays just after shedding. Fig. 1 shows the mean SSH of 11 Agulhas rings as a function of age (only rings that live longer than 30 months were taken into account) obtained by Schouten et al. (2000), plus standard deviation. (It also shows the decay of SSH of Ring Astrid which we discuss below.) During the first 5 months the average SSH decay is fast: 5 cm per month. After 10 months the rings decay very slowly: 0.5 cm per month. The early, fast decay phase coincides with the rings crossing the Benguela Current. So, it is argued that the mixing process(es) associated with the fast decay phase probably determine(s) the proportion of Agulhas leakage that contributes to the upper branch of the THC. Assuming that the decay of SSH coincides with decay of density anomaly, the density anomaly associated with the rings is to a large extent mixed away into the surroundings during the fast decay phase.

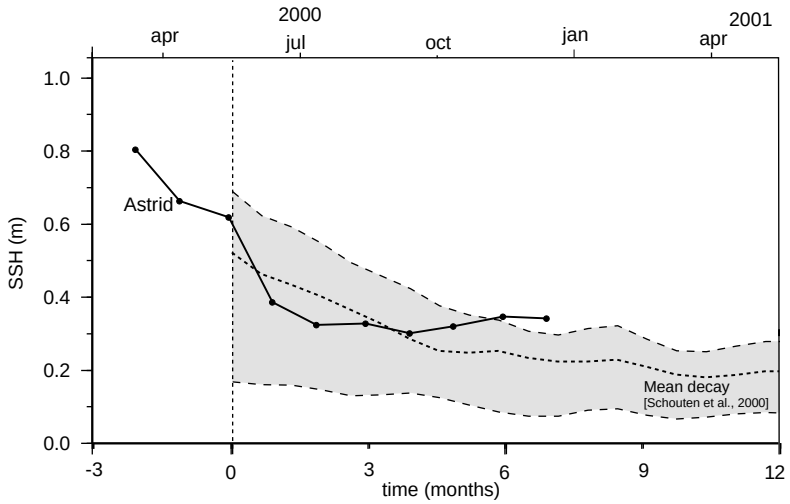

Fig. 1. SSH of ring Astrid as determined from TOPEX-POSEIDON altimetry plotted against age (courtesy M. Schouten), together with mean SSH and bars of 1 standard deviation of 11 Agulhas rings plotted against their age from Schouten et al. (2000). The *x*-axis displays time in months; the *y*-axis SSH in *m*.

In Autumn 1999, the Netherlands consorted observational and modeling program Mixing of Agulhas Rings Experiment (MARE) started (Lutjeharms et al., 2000). The main goal is to estimate the proportion of Agulhas leakage that contributes to the upper branch of the THC and to identify the dominant mixing processes that determine that proportion. MARE consists of a hierarchy of modeling efforts to support the observational program. Here, we report on a series of model simulations initialized with a circular symmetric, equivalent barotropic idealization of ring Astrid, which was measured during the first MARE-cruise (Van Aken et al., 2003). The survey of Astrid occurred in an early stage of the ring's life, some 2 months before Schouten et al. (2000) would have started monitoring. So, the initial point of the decay-curve of Astrid is displaced with respect to the starting point of the mean decay of Agulhas rings obtained by Schouten et al. (2000) in Fig. 1. The decay of Astrid is not atypical. It is clearly characterized by a fast decay phase during the first 4 months, followed by an almost stationary SSH.

From previous literature the two mechanisms identified for ring decay in numerical models are Rossby-wave radiation and friction. In general, quasi-geostrophic (QG) models feature too strong Rossby-wave radiation from the rings (McDonald, 1998). The propagation speed of the center of mass of QG rings is equal to that of the baroclinic Rossby waves. This enables a relatively strong coupling between rings and Rossby waves. For instance, Beismann et al. (1999) show very strong radiation which is the dominant decay mechanism in their QG simulations. In shallow-water models Rossby-wave radiation from anticyclones is smaller. Kamenkovich et al. (1996) stress the importance of the length scale of the ring compared to the Rossby radius of deformation for Rossby-wave radiation. In their model the Rossby-wave related decay was small for Agulhas rings, due to the large length scale of Agulhas rings. Also, when the nonlinearity of the ring increases Rossby-wave radiation decreases. The remaining mechanism, sub-grid scale friction and diffusion is related to the horizontal resolution. In Chassignet et al. (1990) the decay of Agulhas rings was mainly due to friction. They concluded that decay was 4–6 times too fast in their model compared to observations. By decreasing the viscosity by a factor of 6, the decay time doubled. A further reduction of viscosity lead to an unstable integration. A resolution higher than 20 km was recommended for future studies. At higher resolution/lower explicit friction other decay mechanisms can manifest themselves. One main candidate is the instability of Agulhas rings. Unstable modes may deform the ring and lead to cross-frontal circulations and decay.

The linear stability of ocean rings has been studied extensively. For purely baroclinic rings in a two-layer QG setup, both Flierl (1988) and Helfrich and Send (1988) showed that wide (with respect to the Rossby deformation radius) ocean rings are more unstable than narrow rings. The wavenumber of the most unstable mode increases with increasing ring diameter, a feature that is also observed in laboratory experiments (Saunders, 1973). Similar results were derived in studies considering large clouds of point vortices (e.g., Hogg and Stommel, 1985) The presence of a corotating barotropic component was found to be able to stabilize ocean rings (Helfrich and Send, 1988; Flierl, 1988). More recent studies of ocean rings in a shallow-water context (Dewar and Killworth, 1995; Killworth et al., 1997) confirmed this. For the Gaussian and cubic radial profiles that were studied, the growth rates of the most unstable modes in the corotating regime are an order of magnitude smaller than in the counter-rotating regime. The finite-amplitude evolution of the rings was generally in agreement with the linear predictions (Dewar et al., 1999). Katsman et al. (unpublished data, hereafter K02) show that the sharp contrast between co- and counterrotating rings is a consequence of the choice for a weakly declining radial velocity profile. For steeper, more realistic profiles the rings become more unstable and the growth rates of co- and counterrotating rings become of the same order. Rings with a weak deep flow become the least unstable. This holds also for a four-layer idealization of ring Astrid whose nonlinear evolution is studied in the present paper.

In the present study we aim to model the observed SSH decay of Astrid, and in particular

the fast, initial decay phase in a parameter regime where the friction and viscous dissipation are too weak to impact the modeled SSH. Also, we want to identify the dynamical process(es) responsible for the fast, initial decay and to comment on the generality of the results by performing a parameter sensitivity study.

2. Experimental setup

The numerical simulations were performed with MICOM 2.7, which is an extended version of the ocean general circulation model described by Bleck and Smith (1990). Computations have been carried out on a 201×201 doubly periodic domain (about 1000 km $\times$ 1000 km), with a flat bottom at 4000 m depth. The horizontal resolution is 0.05° (about 5 km) in longitude and latitude and there are 12 layers in the vertical. Lateral diffusion, bottom stress and diapycnal diffusion were set to zero. Lateral friction was according to Bleck and Boudra (1981). No wind and buoyancy forcing was applied, unless otherwise stated. All runs are spin-down experiments, but the time evolution is completely determined by the interior dynamics and viscous dissipation is negligible on the time-scales considered here.

The model was initialized with a circular symmetric, equivalent barotropic idealization of ring Astrid, measured during the first MARE-cruise (February 27, 2000–March 19, 2000). Its center was located near 18.5°E and 38.0°S. Two long sections were taken through the ring of 19 stations each, with an interval of 20 km. Nine stations were taken to the bottom, otherwise to 1000 m depth. Two additional shorter sections were taken to improve the coverage of the ring's edge (see Van Aken et al., 2003, for more details). Fig. 2a shows the potential density referenced to the surface, σ_0, as a function of depth for one cross section through Astrid. The data from this and the other sections were spatially averaged with respect to distance from the ring center to obtain a circular symmetric radial profile.

The idealized radial profile used for the simulations is defined based on the shape of the density surface at 50 m outside the ring (the bottom of layer 1 in the model). The depth of this density surface was assessed as a function of the radial distance from the ring center. This curve could be approximated by a parabolic profile inside the ring (solid body rotation), and an $\exp(-r^4)$ profile outside the ring. The bounding edge between inside and outside was defined by the position of the velocity maximum of the ring and will be denoted by R. For ring Astrid $R = 130$ km. The standard radial profile then becomes

$$(h_j)(r) = (h0_j)(1 - (r/R)^2/2), \quad r < R, \tag{1}$$

$$(h_j)(r) = (h0_j)/2 \exp((1 - (r/R)^4)/2), \quad r > R. \tag{2}$$

Fig. 3a displays this fit together with three other profiles and shows that our standard profile collapses on the data better than the exponential profiles. In Section 4 we will comment on the sensitivity of the numerical results to the chosen radial profile. The same profile was used for all layers; the amplitude was obtained by evaluating the σ_0 values at the undisturbed layer depths outside the ring, and then calculating the depth of this σ_0 level at the ring center.

We thus assume an equivalent barotropic structure. The measurements show that this assumption is well met in the upper 2000 m (Van Aken et al., 2003). Below 2000 m, the ring is slightly deformed by interaction with the bottom topography. Since we start with the more general flat bottom domain, the equivalent barotropic structure seems justified. Both velocity and density measurements indicate that the ring extends to the bottom. To account for this, we assume a barotropic pressure gradient that overcompensates the baroclinic pressure gradient in the deepest layer, so that the ring is corotating. The initial velocity field was obtained by demanding cyclo-geostrophic balance. The maximum velocity in the upper layer is 0.88 m s^{-1}; in the deepest layer it is 0.16 m s^{-1} which compares well with the observations. The associated SSH signal is 0.75 m, slightly less than the 0.8 m estimated from the altimetry data (Fig. 1). The maximum barotropic velocity is 0.3 m s^{-1}. Fig. 2b shows the initial radial profile for layer depth; Fig. 3b for velocity.

We have used periodic boundary conditions in both E–W and N–S directions. Due to the periodic

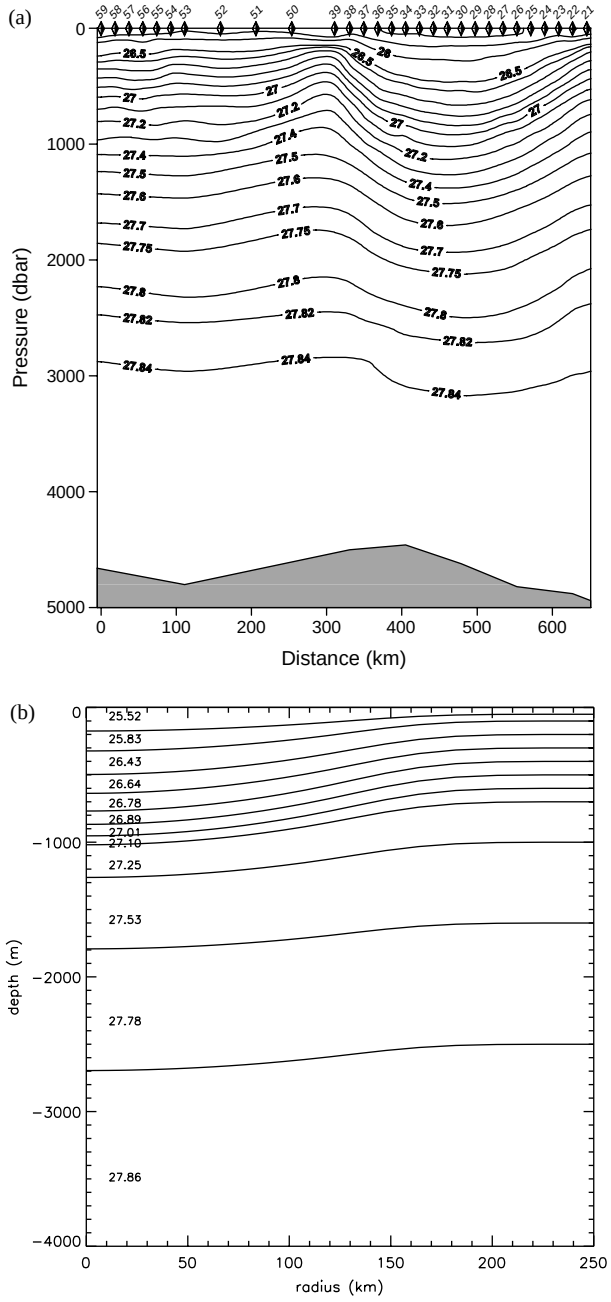

Fig. 2. (a) CTD-section of potential density through ring Astrid and outer-ring area, as obtained during MARE-1. (b) Section of layer interfaces as a function of depth and distance from center for the idealization of Astrid. Potential density is given for each layer.

boundary conditions there is a jump in f and thus in potential vorticity at the north/south boundary. This mostly affects the barotropic waves that reenter the domain across this boundary. The impact of this distortion of the barotropic wave field on the ring itself seems to be small and not to affect the evolution characteristics of the ring.

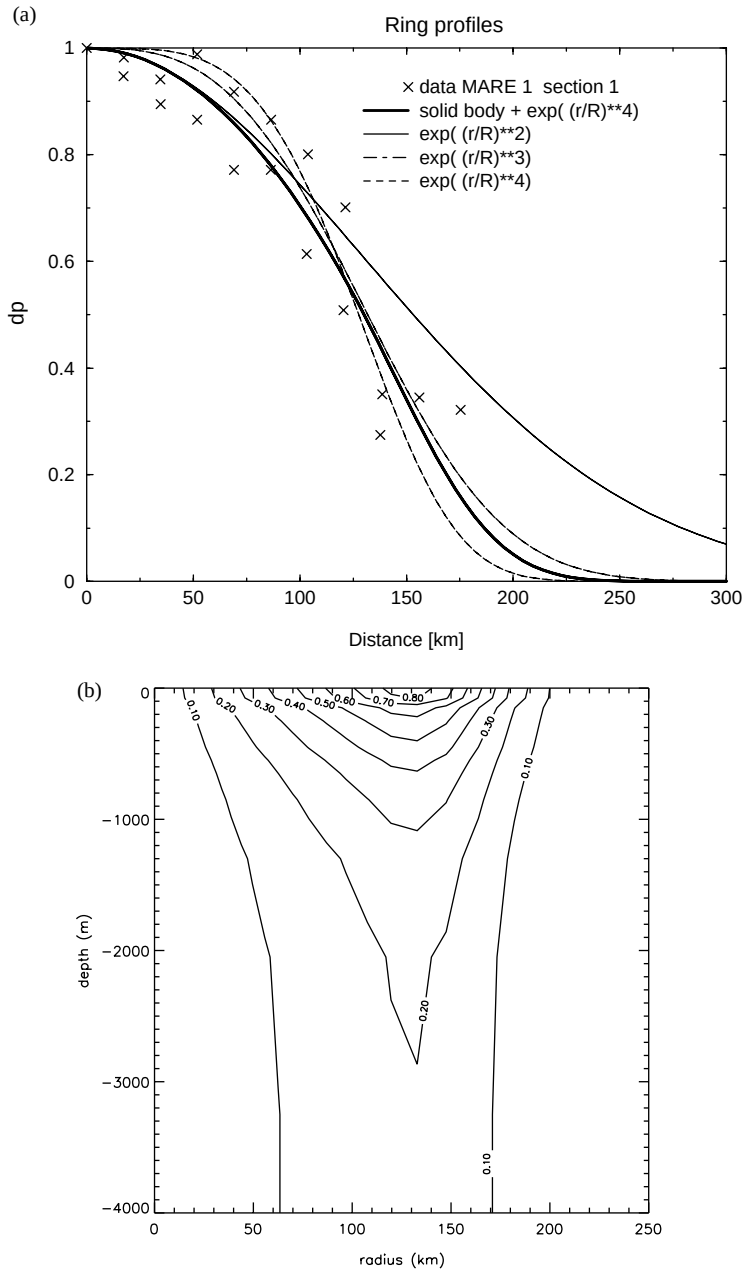

Fig. 3. (a) Initial radial profile of (scaled) upper layer depth as a function of distance from center. Crosses denote measurements. The thick solid line is the standard profile. (b) Section of velocity as a function of depth and distance from center for the idealization of Astrid. Contour interval is 0.1 m s^{-1}.

3. Linear stability and time evolution of Astrid

3.1. Stability analysis

Ripa (1989) derived necessary conditions for instability for axisymmetric ocean rings on an f-plane, in an N-layer shallow-water setup. According to these criteria, which depend on the radial velocity, the potential vorticity gradient and the density profile of the ring, the standard radial profile of Astrid is possibly unstable. Based on its size with respect to the Rossby deformation radius and the fast declining velocity profile, the linear analysis of Flierl (1988) also predicts this ring to be unstable. To gain more insight in the time evolution of the ring we analyzed its linear stability, using a 12-layer shallow-water model on an f-plane (see K02 for details on the model and method). We consider the stability of the idealization for Astrid with respect to infinitesimally small perturbations of the form ($j = 1, \ldots, 12$)

$$(u_j, v_j, h_j)(r, \theta, t) = \mathrm{e}^{(\sigma_r + i\sigma_i)t + im\theta}(\tilde{u}_j, \tilde{v}_j, \tilde{h}_j)(r) \qquad (3)$$

with growth rate σ_r, period $2\pi/\sigma_i$, integer azimuthal mode number m and spatial pattern $(\tilde{u}_j, \tilde{v}_j, \tilde{h}_j)(r)$. Substitution of (3) in the linearized momentum and continuity equations yields the linear stability problem, depending only on the coordinate r and the azimuthal mode number m.

Despite the presence of a strong barotropic component ($V_{12} = 0.16$ m s^{-1}) that may induce a stabilizing effect (Helfrich and Send, 1988; Flierl, 1988; Dewar and Killworth, 1995), the linear stability analysis shows that this standard profile is unstable with respect to an $m = 2$ mode. Only the spatial pattern of the perturbation at the first interface, h_2, is shown in Fig. 4a; the mode has an equivalent barotropic structure. The growth rate of this mode is 0.11 day^{-1}, and its period is 49 days. The ring is also unstable with respect to an $m = 3$ mode, with a growth rate of 0.09 day^{-1} and a period of 25 days (Fig. 4b). For both modes, the maxima of the perturbations are located on the outer flank of the ring. The instability has a mixed baroclinic/barotropic character.

We checked whether the time evolution of the ring during the initial growth phase of the instabilities is correctly predicted by the stability analysis. The time evolution of the perturbation in the f-plane simulation is monitored by subtracting the initial thickness field from the instantaneous thickness at various stages of the time integration. The anomalous upper layer thickness is shown in Fig. 5 for day 5 and 40, which should be compared to the anomalous interfaces shown in Fig. 4. The anomalous upper layer thickness in the time integration displays a pattern with two maxima and two minima, although during the first 10 days it is not symmetric yet (Fig. 5a; day 5). As this perturbation grows, it resembles the calculated pattern of the $m = 2$ mode more and more (Fig. 5a; day 40). Also, in the deeper layers the perturbation is very similar to the pattern of

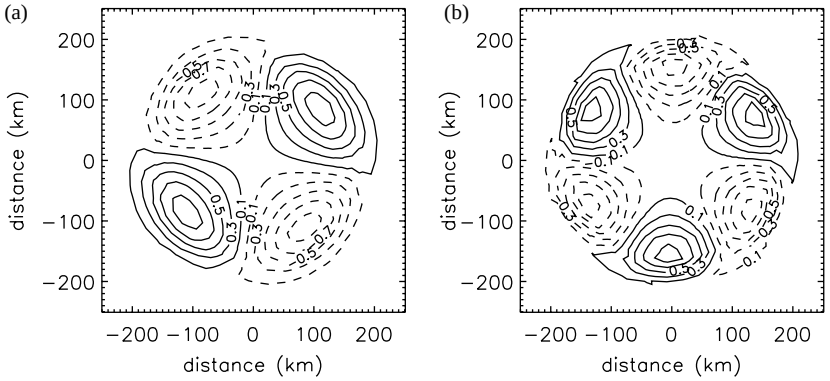

Fig. 4. Normalized perturbation depth of the first interface h_2 of (a) the $m = 2$ and (b) the $m = 3$ mode for the standard case, scaled with their maximum (contour interval is 0.2). The quantity on the x- and y-axis is distance from center in km.

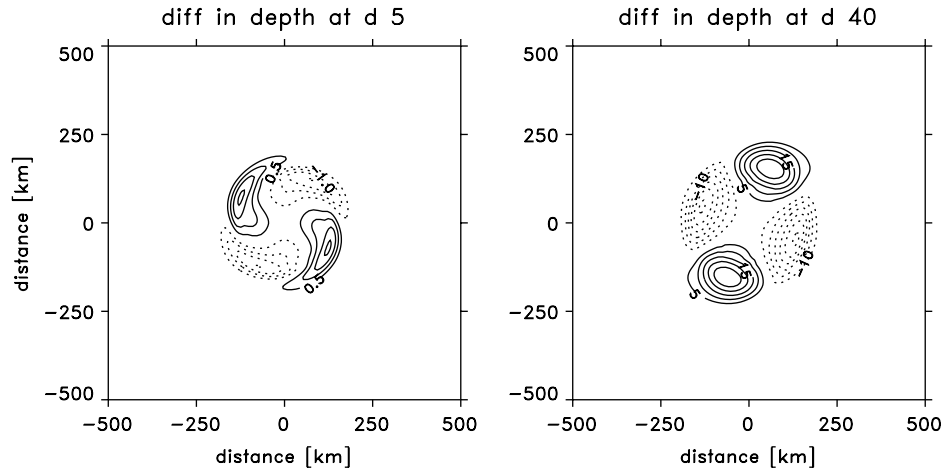

Fig. 5. Upper layer thickness anomaly relative to the initial profile for the time integration on the f-plane, at day 5 and 40. Contour interval is 2 m.

layer 1, in agreement with the equivalent barotropic structure. Apparently, the growth of the $m = 3$ mode does not play a role in the early evolution of the ring. Its initial evolution seems to be governed by the growth of the most unstable mode derived from the linear stability analysis, in agreement with earlier studies of ring evolution (e.g., Helfrich and Send, 1988; Dewar et al., 1999).

3.2. Ring evolution

Our standard experiment is a numerical integration of ring Astrid on the β-plane. (All numerical simulations have been performed on the β-plane, except one f-plane run; all linear stability analyses have been performed on the f-plane.) The change in planetary potential vorticity (PV) gradient over the ring is typically only 2% of the PV anomaly in the upper layer. Therefore, β is unimportant in the early evolution of the ring (linear phase) and its linear stability characteristics. Fig. 6 shows the evolution of upper layer thickness. During the first 30 days the ring moves westward due to the β-effect (not shown). Consistent with the linear stability analysis of Section 3.1 the ring is unstable to an $m = 2$ mode perturbation, which causes it to become elliptic. At day 30 the $m = 2$ perturbation has attained a significant amplitude and the evolution becomes more nonlinear. Lobes at the extremes are developing. The ring starts moving in a more northerly direction from day 30 onwards. At day 40 the ring has become strongly ellipsoidal and significantly asymmetric. It attains a pear-shaped form. At day 60 the ring has shed off a weaker anticyclone, while the parent ring remains unstable. There are still sizeable lobes that precurse further small-scale shedding events. At day 100 the parent ring elongates again due to a similar $m = 2$ perturbation as seen in the early evolution. At day 120 a second larger shedding event occurs. There are more shedding events to follow and at day 180 the parent ring has been split into 4 larger and 8 smaller parts. The largest ring (250 km north of the center), still has a deep core. The depression of the first interface has changed from 120 m at the start to 100 m at the end of the integration.

During the second MARE-cruise (July 20, 2000—August 9, 2000, some 5.5 months after the first cruise), ring Astrid appeared to be very elongated. It featured a double-core structure and a thin neck of about 20 km wide (Drijfhout, pers. com.). In the second half of the cruise the ring was revisited after taking some geological stations outside the ring. At this time the neck seemed to be broken. These observations are consistent with the scenario of a growing $m = 2$ mode. In reality, however, the evolution of Astrid was also strongly governed by interactions with other cyclones and anticyclones and possibly also

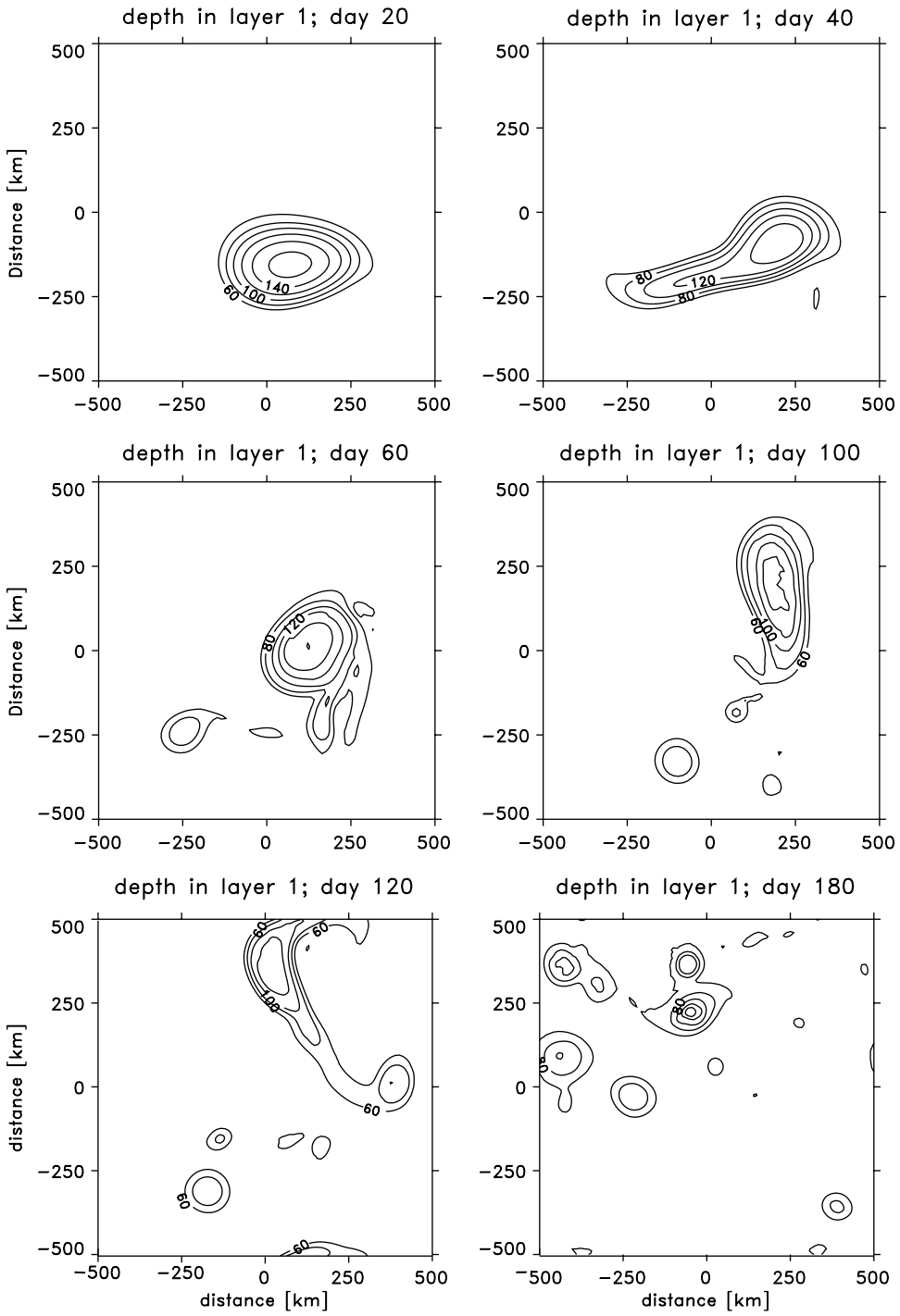

Fig. 6. Upper layer thickness at day 20, 40, 60, 100, 120 and 180. For the standard experiment on the β-plane. Contour interval is 20 m.

with the Agulhas Current itself. As a result, the splitting of ring Astrid cannot be determined in an unambiguous way. Satellite altimetry suggested it was cut through by a westward traveling cyclone during the second MARE-cruise. However, before this splitting occurred the ring seemed to have merged with another anticyclone. As a result, the apparent splitting was associated with the repulsion of the formerly merged anticyclone.

3.3. SSH decay

The calculated SSH as a function of time (Fig. 7) shows that the modeled decay (thick solid line) recovers an initial, fast decay phase consistent with the fast decay phase shown in Fig. 1 (dotted line), albeit with stronger decay. Fig. 1 suggests a 120 days (4 months) time-scale for the initial, fast decay. The modeled decay in the initial phase is from 75 to 36 cm, or 10 cm/month. Thereafter SSH increases with 1 cm/month. The mean initial SSH decay of Agulhas rings as given by Schouten et al. (2000) is from 52 to 28 cm (dotted line), or 6 cm/month, but their curve starts indicating SSH approximately 2 months after the moment that ring Astrid was surveyed by the first MARE-cruise. If we (linearly) interpolate their mean decay curve back in time to coincide its starting point with the first MARE-cruise, using the decay rate of the first 15 days (8 cm/month), mean decay would be 7 cm/month (dashed line). The observed decay of Astrid as estimated from satellite altimetry is from about 80 to 33 cm in the first 120 days (thin solid line), or 11.75 cm/month. Overall, there is a good correspondence between the modeled and observed decay in SSH. The modeled curve is more capricious, associated with the various shedding and splitting events. On the other hand, the altimetry algorithm strongly smoothes variations in time. Since the modeled time evolution is dominated by the growing $m = 2$ perturbation, the results suggest that the instability process is responsible for a large part of the observed decay. The robustness of this result will be further investigated in the next section with a parameter analysis.

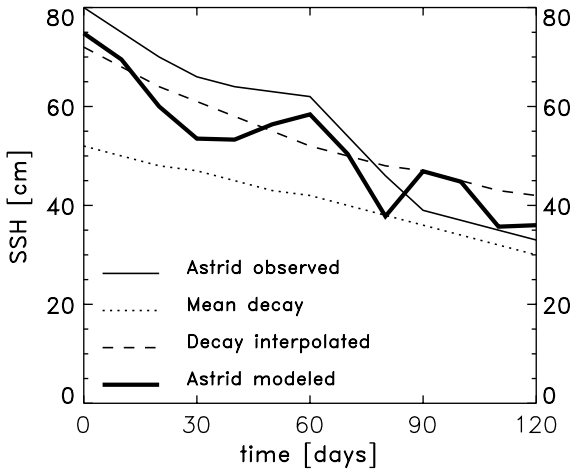

Fig. 7. Observed (thin solid line) and modeled SSH decay (thick solid line) for Astrid as a function of time, together with the mean decay curve from Schouten et al. (2000) (dotted line), and the same curve interpolated back in time for 2 months (dashed line).

4. Parameter analysis

A series of numerical experiments was performed to investigate the effects of ring strength, diameter, barotropic structure, cooling and β on decay, to assess whether the SSH decay indeed can be associated with the instability of the ring. Also, the sensitivity of the results to the use of different ring profiles was tested. In the first set of experiments we relate the ring strength to a parameter α that indicates the interface displacements and barotropic pressure gradient relative to those in the idealized profile of ring Astrid. In the additional experiments where other parameters are investigated the ring strength will remain constant at $\alpha = 1$.

4.1. Ring strength (α)

The influence of ring strength α on the stability of the ring is investigated. Even though the stability problem does not depend linearly on α, decreasing α results in an almost linear decrease in growth rate and increase in period, for both the $m = 2$ and 3 mode in the linear stability analysis. However, the ring remains unstable for all values of $\alpha > 0$. This is consistent with the results of

Benilov et al. (1998), who showed that all geostrophic large-amplitude vortices are unstable, regardless their profile and stratification. Also, nearly all ageostrophic vortices they considered appeared to be unstable. Only when the radius was sufficiently decreased leading to Rossby numbers of at least 0.3, stable vortices could be found. For $\alpha = 0.4$, the weakest ring discussed here, the $m = 2$ mode is still dominant, and has a growth rate $\sigma_r = 0.040\ \text{day}^{-1}$, the growth rate of the $m = 3$ mode is only slightly smaller ($\sigma_r = 0.036\ \text{day}^{-1}$). In general, the difference in growth rate between the $m = 2$ and 3 modes decreases with decreasing α, but the $m = 2$ mode remains the most unstable.

The same impact of α on wave growth is recovered by the time integrations; decreasing α causes the growth of the $m = 2$ mode to slow down. The anticyclone eventually shed-off, however, becomes larger. When α is decreased to 0.6, the shed-off anticyclone is large enough to split itself again, with one part reattaching to the parent ring. When α is decreased beyond 0.5, the ring no longer splits, although its nonlinear evolution is still determined by the growth of the $m = 2$ perturbation. Fig. 8 shows the scaled decay of SSH as a function of α. During the first 15 days the scaled decay is equal for all values of α. Thereafter, the decay for $\alpha = 0.4$ levels off. The scaled decay increases with increasing instability. This supports our earlier conclusions that the decay of SSH is associated with the instability and splitting of the ring.

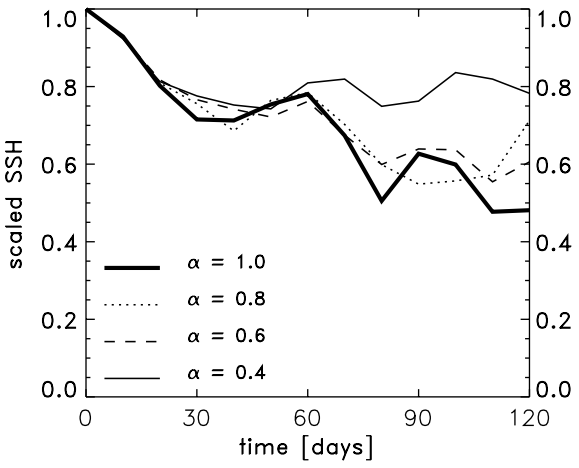

Fig. 8. Scaled SSH decay as a function of ring strength α.

4.2. Radial profile

In addition to the standard solid-body profile, exponential profiles were considered:

$$(h_j)(r) = (h0_j)\exp(-(r/R)^n), \quad n = 2, 3, 4. \tag{4}$$

From Fig. 3 it is seen that the exponential profile with $n = 2$ falls off too slowly near the ring's edge, which causes a larger signal outside the ring. Exponential profiles with higher exponents fall off too slowly near the ring's core, but feature a steeper decline near the ring's edge. For all exponents considered the two most unstable modes were found to be an $m = 2$ and an $m = 3$ mode. Increasing the exponent enhances the instability of the ring, as can be expected for the associated increase in the basic state velocity and its shear (the growth rate of the $m = 2$ ($m = 3$) mode increases from 0.013 to 0.13 day^{-1} (0.010 to 0.11 day^{-1})). The stability characteristics of the exponential profile with $n = 4$ are comparable to those of the standard solid body profile, which also has a fourth-order decay outside its core. Since the most unstable modes act on the ring's outer flank (Fig. 4), it is not surprising that the steepness of the velocity profile determines the stability. A similar result was obtained by K02.

In the time integrations multiple split-up occurs in all cases. The ring with $n = 2$ first splits into two large parts, which subsequently split-up in smaller parts. The other rings feature consecutive shedding off of smaller anticyclones. Elongation develops faster when the exponent of the profile increases but much less spectacular than the linear stability analysis predicts. The scaled decay in SSH is for all radial profiles rather similar during the first 60 days (Fig. 9). Thereafter, the decay-curves start oscillating, as, after splitting, SSH may temporarily increase during an adjustment phase, after which SSH decreases again if the instability process still determines the further evolution of the parent ring. These experiments suggest that the details of the radial profile are not very critical for the early evolution of the ring, which in all cases is determined by the development of an $m = 2$ mode,

but become more important for the nonlinear evolution of the ring.

4.3. Diameter

The linear stability of ocean rings is found to depend critically on the ratio of their diameter and the internal Rossby deformation radius (Flierl, 1988; Helfrich and Send, 1988): larger rings are found to be more unstable. In addition, the dominant wavenumber for which the rings become unstable increases with increasing diameter (Hogg and Stommel, 1985; Saunders, 1973).

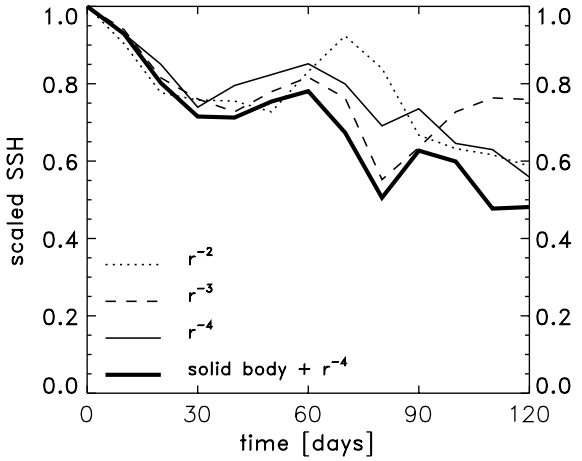

Fig. 9. Scaled SSH decay as a function of radial profile.

Both the radius at which the velocity maximum occurs and the width of the declining velocity profile on the ring's outer flank are of importance. The standard profile used in this study ($R = 130$ km; while the internal Rossby deformation Radius is 28 km) violates the stability criteria derived by Flierl (1988) for QG ocean rings: decreasing (increasing) the characteristic diameter R of the ring will increase (decrease) the steepness of the velocity profile on the ring's outer flank and is thus expected to enhance (reduce) its instability. Our linear stability analysis indeed shows a monotonous increase in growth rate of the dominant $m = 2$ mode from 0.08 day^{-1} for $R =$ 160 km to 0.18 day^{-1} for $R = 90$ km.

The nonlinear behavior shown in the time integrations is far more complex. Increasing R to 160 km indeed leads to weaker growth of the $m =$ 2 mode compared to the standard run, in agreement with the linear predictions. Eventually the ring splits into various smaller anticyclones. When R is decreased to 110 km the ring also splits in various smaller ones, but the growth of the $m =$ 2 mode again develops slower than for the standard run, contrary to the linear stability analysis. Decreasing R further to 100 km causes the growth of the $m = 2$ mode to become even slower, but now the ring splits almost perfectly in two similar halves (Fig. 10). With $R = 90$ km the ring appears to stabilize after some initial linear

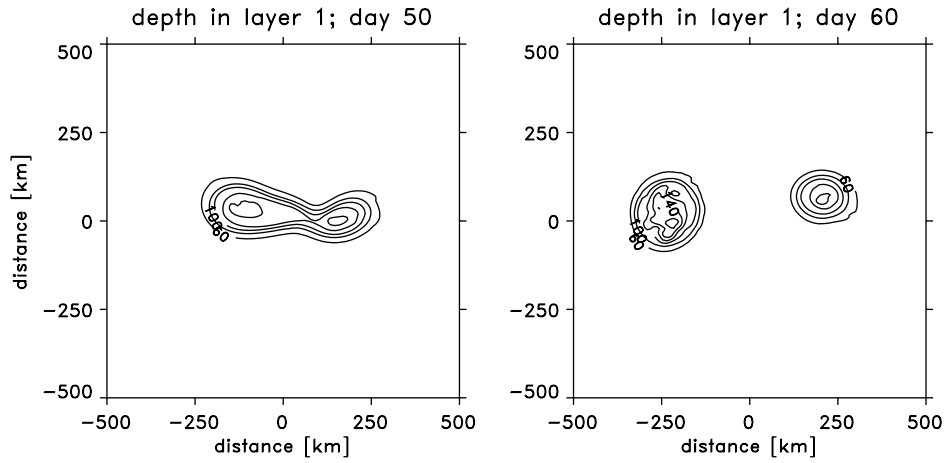

Fig. 10. As Fig. 6, but now for $R = 100$ km, and day 50 and 60.

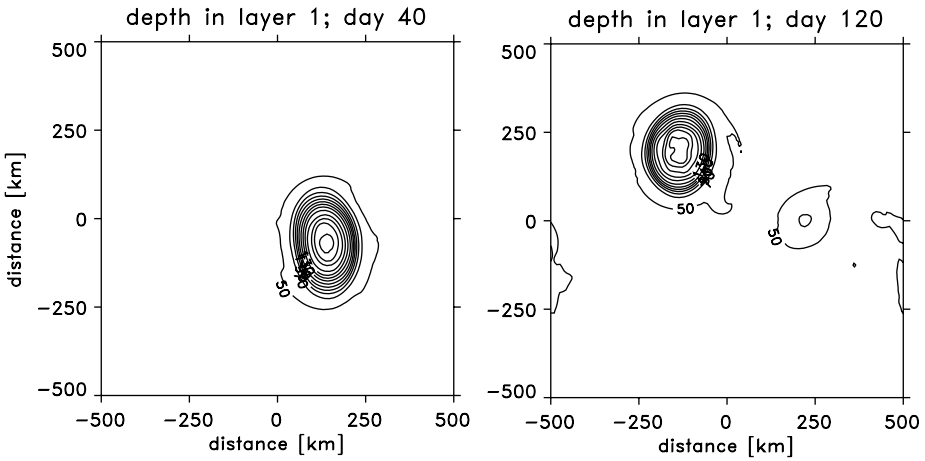

Fig. 11. As Fig. 10, but now for $R = 90$ km, and day 40 and 120; contour interval is 10 m.

growth of the $m = 2$ mode, see Fig. 11. Between day 40 and 120 the ring remains coherent and evolves from an elliptic shape back to a circular form. Note that R still is much larger (three times) than the Rossby radius of deformation. The fact that it nearly retains its initial shape is not associated with its linear stability characteristics. Also, frictional dissipation is still too weak to affect the stability of the ring. Benilov et al. (1998) could stabilize warm core vortices when the diameter was reduced to about 2 times the Rossby radius. But they considered compensated eddies with a different radial profile.

An energy analysis of the $m = 2$ mode (see K02 for the procedure) revealed the following. Decreasing the diameter not only increases the linear instability of the ring, also the instability attains a more barotropic character as the barotropic energy gain becomes more dominant. At $R =$ 90 km the baroclinic energy conversion becomes even negative; from the $m = 2$ mode back to the parent ring. At the same time the $m = 2$ mode itself becomes more barotropic; the ratio of layer depth anomaly to SSH becomes smaller. Apparently, the growth of this $m = 2$ mode does not lead to split-up. Rather, the ring initially evolves to a tripolar state where it is accompanied by two barotropic cyclones. Later on, its appearance becomes more complex. In a two-layer model Dewar et al. (1999) showed an example for which the splitting of an anticyclone was suppressed when the ring had a substantial barotropic component, and that the final equilibrated state is tripolar. Laboratory experiments indicate that such tripolar states are very stable (Kloosterziel and Van Heijst, 1989). It seems that only when the growth of the $m = 2$ mode is associated with a substantial baroclinic energy conversion, the growth of the $m = 2$ mode leads to split-up. The $m = 2$ mode always has a barotropic component in our time integrations, visible in SSH as time evolves. But the baroclinic component of the $m =$ 2 mode almost disappears when R becomes smaller than 100 km. This is probably associated with the fact that in all cases we considered there is a positive barotropic conversion from the parent ring to the $m = 2$ mode, while the baroclinic conversion becomes negative for $R < 100$ km. For $R = 90$ km the $m = 2$ mode is invisible in the patterns of layer depth. Fig. 12 shows the SSH patterns of this mode for $R = 90$ km at day 40 and 120, which can be compared to the patterns of upper layer depth in Fig. 11. Fig. 12 confirms the almost purely barotropic nature of the $m = 2$ mode. These experiments suggest that it is not the linear stability of the ring that determines its fate with respect to elongation and splitting but the baroclinic energy conversion involved with the instability. When the barotropic energy conversion is dominant the ring equilibrates in the nonlinear

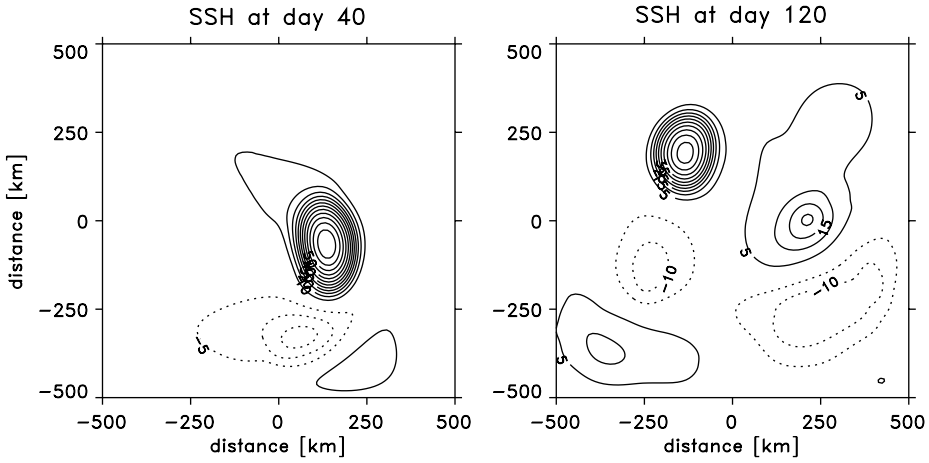

Fig. 12. As Fig. 11, but now for SSH. Contour interval is 5 cm.

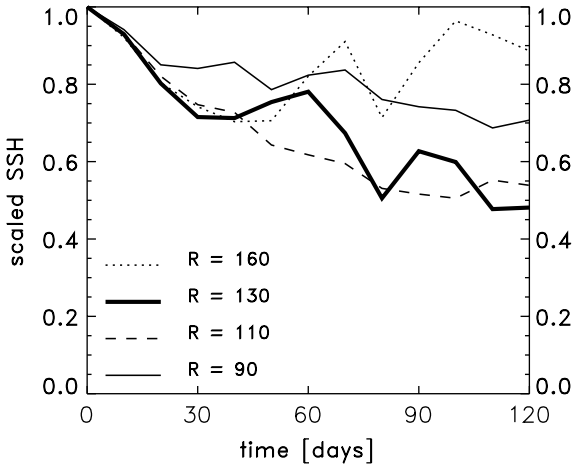

Fig. 13. Scaled SSH decay as a function of diameter R in km.

phase long before splitting. A tentative explanation is that the barotropic energy conversions, which are largest around the radius where the horizontal shear of the basic state is at its maximum, act to reduce the horizontal shear of the ring so that the ring's barotropic instability is decreased as it evolves.

In accordance with the results discussed above the scaled decay in SSH for $R = 160$ km oscillates vigorously and is less than for the standard profile; for $R = 110$ and the standard run the scaled decay is largest; for $R = 90$ km the decay levels off quickly and is the smallest (Fig. 13).

4.4. Barotropic component (ψ)

Both in a QG (Flierl, 1988; Helfrich and Send, 1988) and a shallow-water context (Dewar and Killworth, 1995; Dewar et al., 1999) it was shown that a corotating barotropic component has a stabilizing effect on ocean rings, provided that this barotropic component itself is not unstable. K02 showed that realistic rings, like their idealization of Astrid, do have an unstable barotropic component. That is, corotating rings are barotropically unstable, whereas counterrotating rings were found to be mainly baroclinically unstable. In between is a regime of nearly compensated rings (with weak subsurface flow) that feature the smallest growth rates. The barotropic component is measured by ψ, with $\psi = 1.0$ indicating a compensated ring with zero velocities in the lowest layer; the idealization of Astrid has $\psi = 1.25$. A linear stability analysis of two cases with a weaker barotropic component than the standard profile ($\psi = 1.0$ and 0.75) confirms the earlier results of K02. The compensated ring ($\psi = 1.0$) has the smallest growth rate (0.08 day^{-1} versus 0.11 day^{-1} for the standard case). For the compensated and corotating rings the $m = 2$ mode is always dominant. For the counterrotating ring ($\psi = 0.75$), the $m = 3$ mode becomes dominant. Its growth rate is 0.09 day^{-1}.

The time integrations indeed show most vigorous wave growth for the counterrotating ring.

Contrary to the linear stability analysis, growth of the $m = 2$ mode dominates the nonlinear phase and the ring splits in two, almost equal, halves. The compensated ring indeed shows weaker growth of the $m = 2$ mode than in the standard run. Splitting occurs later and the newborn anticyclone is larger than observed for the standard run. Afterwards there is some further shedding of much smaller anticyclones, but the evolution is characterized by one major splitting event. Increasing the barotropic component further makes the ring more barotropically unstable. In the former section we saw that for $R = 90$ km the ring could be stabilized in the nonlinear phase when the horizontal shear associated with the barotropic instability became sufficiently strong. A larger ring can have the same horizontal shear by increasing the barotropic component ψ. For $R = 130$ km a similar equilibration by increasing ψ does not occur. With $\psi = 1.8$ the growth of the $m = 2$ mode is indeed halted at day 30. Thereafter, small anticyclones are shed off at day 50 and 80. From day 100 onwards the parent ring starts elongating by the growth of the $m = 2$ mode and splitting occurs at day 150. The ring seems to adjust itself towards a basic state in which baroclinic energy conversions slowly become more important. As a result of this adjustment, the unstable $m = 2$ mode gradually attains a more baroclinic character and the baroclinic energy conversion starts growing from day 100 onward. A similar scenario occurs when the barotropic component is increased further. In the two-layer results of Dewar et al. (1999) anticyclones with a strong enough barotropic component could evolve towards a tripolar state that consisted of the parent ring plus the initial barotropic $m = 2$ mode equilibrated at modest amplitude. In our experiments this state is not as stable as the results of Dewar et al. (1999) suggest. It should be noted, however, that our rings are larger than those considered in Dewar et al. (1999). As the ring with $R = 90$ km remained closer to this tripolar state than the ring with $R = 130$ km it could very well be that this tripolar state is more stable for smaller ring diameter.

The scaled decay in SSH shows surprising behavior (Fig. 14). The corotating rings decay strongly. The compensated ring oscillates with hardly any net decay. The counterrotating ring features increasing SSH. This suggests that growth of the $m = 2$ mode is associated with an interaction between the barotropic and baroclinic components within the parent ring, such that the ring attains a nearly compensated structure. Rings with $\psi < 1.0$ feature an increase of the barotropic component, while rings with $\psi > 1.0$ feature a decrease of the barotropic component, and subsequently a decay in SSH.

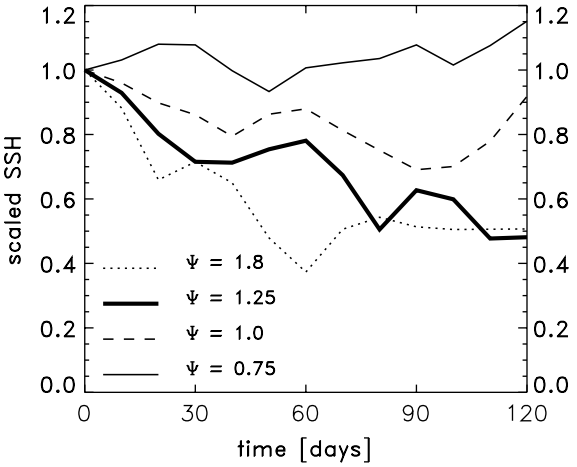

Fig. 14. Scaled SSH decay as a function of the barotropic component ψ.

4.5. Cooling

The initial fast decay of Agulhas rings, just after shedding, coincides with the strongest heat loss. Therefore, we also investigated the impact of cooling on the ring evolution. For realistic buoyancy losses the impact appears to be weak. In case of Agulhas rings, the stratification is rather strong and the depth penetration of the effect of cooling is small. As a result, the Rossby radius is hardly changed by convection (a few percent) and the dominant effect is the reduction of vertical shear in the upper layers. As a consequence, cooling slightly stabilizes the ring and the instability process develops marginally slower.

5. Discussion

5.1. Decay processes: energy conversions and mass exchange

The decay of SSH may be associated with the weakening and spreading of the ring, without any exchange of water between the ring and its surroundings. We studied the basin averaged energy budgets to gain some insight into the processes associated with the SSH decay in the standard run. The basin integrated kinetic energy increased until day 160, after which it decreased again. As a consequence, the ring evolution is characterized by a conversion from available potential to kinetic energy, with a marginal role for frictional decay (this is true for all runs discussed here). Fig. 15 shows that the increase of kinetic energy is completely due to an increase of the barotropic flow (dotted line), while the baroclinic kinetic energy (here defined as total kinetic energy minus kinetic energy of the barotropic flow) slightly decreases (dashed line). This implies that the flow becomes more barotropic in time.

For the parent ring itself this is not true. Fig. 15 shows that SSH (thick solid line) decays faster than the thermocline depth anomaly (thin solid line). Within the parent ring there is an energy transfer from the barotropic to the baroclinic components, and the parent ring becomes more baroclinic when it evolves in time. This can only be reconciled with the total flow becoming more barotropic if the various modes, growing through the instability of the parent ring, become more barotropic than the ring itself. So, SSH decay of the ring is associated with a conversion from available potential energy of the ring to kinetic energy of nearly barotropic higher order modes.

The ring was initialized with a passive tracer within its core (defined as the region where the initial interface displacement is $> 5\%$ of the maximum anomaly), to illustrate the exchange of water between ring and surroundings. Within the core tracer values were set to 1, outside they were 0. We kept track of the amount of tracer within the depth contours that initially defined the ring's core. The total loss of passive tracer (dotted line in Fig. 16 scales well with the decay of SSH (solid line)). Within the thermocline loss of tracer is 25% less (dashed line). Mass exchange in the deepest layer is mainly due to dispersion by Rossby-wave radiation. In the thermocline mass exchange preferably occurs at the lobes at the extremes of the $m = 2$ mode perturbation. Tracer loss in the deep layers levels off more quickly than tracer loss in the thermocline.

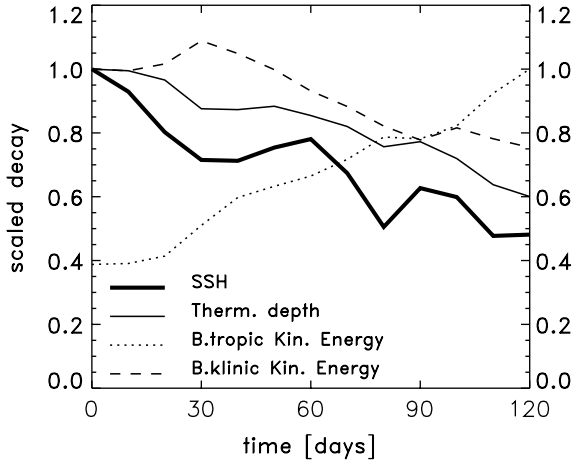

Fig. 15. Scaled decay of SSH (thick solid line), thermocline depth (thin solid line) and basin integrated barotropic (dotted line) and baroclinic kinetic energy (dashed line).

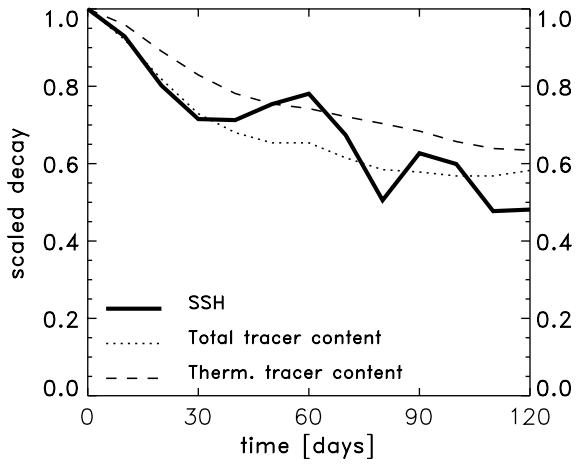

Fig. 16. Scaled decay of SSH (thick solid line), total tracer content (dotted line) and tracer content in the thermocline (dashed line).

5.2. The role of β

Due to its relative smallness β is unimportant in the linear stability of the ring. The initial evolution of isolines of layer depth is rather similar in the β- and f-plane runs (Sections 3.1 and 3.2). To assess the role of β on the nonlinear phase of the ring evolution and on decay of SSH we compare the two runs more extensively. We imposed a small initial perturbation on the SSH and thickness fields in the f-plane run. (Without such a perturbation the ring remains stable on the f-plane, as the linear growth of an infinitesimal perturbation immediately equilibrates with frictional decay. On the β-plane, however, the distortion due to the β-effect is large enough to overcome the effects of friction and an initial perturbation is not needed for the instability to develop.) The result is that ring evolution on the f-plane typically lagged 20 days that on the β-plane. Till day 50 (day 30 on the β-plane) the evolution in (upper) layer thickness fields is very similar. Thereafter growth of the higher order modes on the β-plane becomes asymmetric. Fig. 17 shows the total upper layer thickness for day 60 and 80 on the f-plane just before split-up occurs. It is evident that the ring evolution remains completely symmetric.

Examination of the differences in evolution between the f- and β-plane runs (Figs. 17 and 6) reveals a different evolution of the lobes at the extremes of the $m = 2$ mode in the two runs. In the f-plane run, the development occurs in a symmetric way. In the β-plane run, the symmetry is broken and one lobe (the back-lobe) grows much faster than the other. In the f-plane run mass exchange through the lobes is much less. Also, Rossby-wave radiation is absent.

It is seen that in the initial stage of the f-plane run there is almost no decay (Fig. 18). There is a sudden drop in SSH just before the ring splits, thereafter the decay rate levels off. Apparently, in the nonlinear phase the β-effect plays a significant role in the decay of SSH. The role of β on SSH decay is associated with differences in the energy conversions on the f- and β-plane. First, the conversion from available potential to kinetic energy on the f-plane is 55% of that on the β-plane. Second, there is hardly a net energy conversion from the barotropic to the baroclinic components in the parent ring. For a channel flow, β has a stabilizing effect on the linear (baroclinic) instability. In the nonlinear phase the stabilizing effect of β no longer exists in a large part of the parameter regime (Drijfhout, 1990). For the ring it is not clear how β increases the instability in the nonlinear phase. It should be noted, however, that β induces asymmetries and subsequently, the finite amplitude instability of higher order modes seems to be increased. The f-plane run features splitting into two halves, while the β-plane run is characterized by multiple split events and a break up in

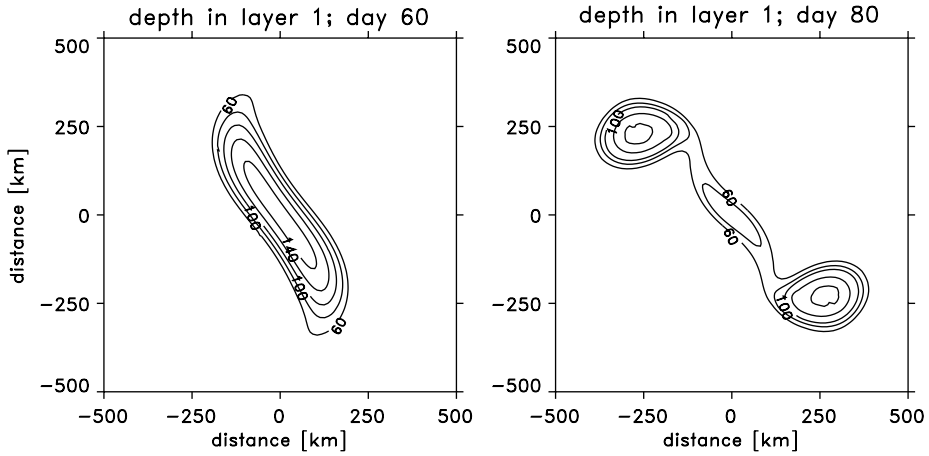

Fig. 17. Upper layer thickness at day 60 and 80 for the f-plane run.

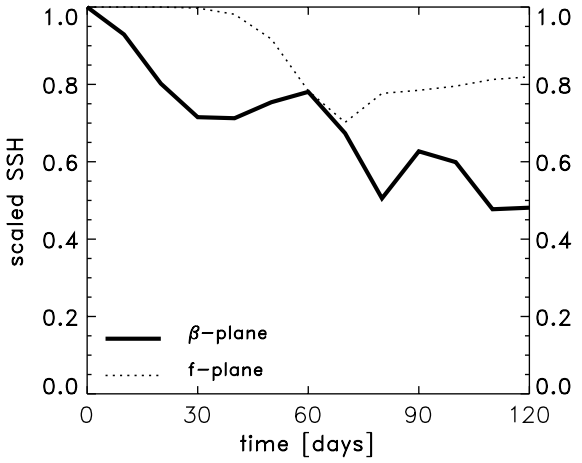

Fig. 18. Scaled SSH decay for the β- (standard) and f-plane runs.

smaller structures. Also, in a reference frame moving with the ring the β-induced movement causes the domain where fluid is trapped into closed streamlines to become smaller. As a result, fluid is much easier stripped off from the core and mixed away with the surroundings.

5.3. Stabilization and splitting

Dewar et al. (1999) found that a barotropic component causing corotation stabilized the rings. In a two-layer version of the model we recover this effect. However, in a multi-layer version (the standard run), keeping the barotropic and first baroclinic mode equal to the two-layer version, the same ring becomes unstable. We did find that a strong enough barotropic component could (temporarily) stabilize the ring in the nonlinear phase ($R = 90$ km and $\psi = 1.8$), because when both the energy conversion and the $m = 2$ mode become dominantly barotropic, equilibration occurs before splitting. Weaker corotating rings, however, can display splitting when the vertical resolution is increased. To understand the details of the differences between the two-layer and multi-layer stability characteristics requires an extended analysis that does not belong in the present paper. We hypothesize that, for the instability to develop for corotating rings, interaction between the barotropic and baroclinic components is required in such a way that most of the rotation and relative angular momentum in the lowest layer is drained off. In all cases the rings seemed to evolve to such a state. In a two-layer version, the lowest layer is often too thick, and the layer integrated rotation too large for this to happen.

The strong tendency of the modeled rings to split is remarkable. Schouten et al. (2000) tracked 20 Agulhas rings using TOPEX/Poseidon satellite altimetry. Of those 20, 6 split-up, and 14 remained coherent. When the splitting is asymmetric, as simulated here, and one of the rings is much smaller, the splitting event can easily be missed by the tracking algorithm used by Schouten et al. (2000). Still, the time integrations suggest more frequent splitting than observed. We note that smaller R and a stronger barotropic component can lead to nonlinear equilibration of the $m = 2$ mode. Also, other factors may come into play that we have not accounted for. For instance (nonlinear) interaction with the background flow, or with other rings and cyclones could prevent splitting. Also, the bathymetry might stabilize the rings. As the splitting process is not essential to the SSH decay, an extensive parameter study to rationalize the tendency for the model rings to split seems out of place here. We have, however, tested the impact of cyclones on the development of the $m = 2$ mode, as the rebound of isopycnals in Fig. 2a and the altimeter data suggest interaction of Astrid with one or more cyclones. Also, Dewar et al. (1999) showed an example of anticyclones that evolved to a tripolar state, consisting of the parent ring and two cyclones. We have not been able, however, to equilibrate the growth of the $m = 2$ mode and to prevent splitting of ring Astrid by initializing it together with one or two cyclones. As there are many degrees of freedom in how to initialize Astrid accompanied by one or more cyclones, the failure of this test is in no way conclusive.

Nof (1990) has argued that anticyclones cannot split, because of an angular momentum constraint, a result at odds with our findings. Splitting requires an increase in rotation to compensate for the increased planetary torque as the newly formed eddies are pushed away from their original center. In our runs we observe an energy

conversion between the barotropic and baroclinic components that is associated with a redistribution of rotation and angular momentum in the vertical. This vertical redistribution of rotation enables splitting. Nof (1990) did not consider the barotropic component of rings in his reduced gravity model. This issue, as well as others discussed above, needs more careful analysis that is beyond the scope of the present paper, and is left for future studies.

6. Summary and conclusions

The initial, fast SSH decay of Agulhas ring Astrid was studied using a high resolution isopycnic numerical ocean model. The initial radial profile we used was a circular symmetric, equivalent barotropic idealization of Astrid, measured during MARE-I as the initial condition. Our objectives were (1) to investigate whether the observed initial SSH decay can be recovered by a numerical model, (2) to identify the dominant processes responsible for the decay, and (3) to comment on its generality by performing a parameter sensitivity study.

It was found that a mixed baroclinic/barotropic instability accounts for most of the observed initial fast SSH decay of this Agulhas ring. In particular, SSH decay is associated with a conversion from available potential energy to kinetic energy. The increase of kinetic energy is associated with the barotropic velocity field. Most of the energy release in the instability process is associated with the growth of an $m = 2$ mode. Although the basin averaged flow becomes more barotropic, the parent ring itself becomes more baroclinic in time. The ratio of thermocline depth anomaly to SSH anomaly increases. This implies that the various modes growing on the instability of the ring are much more barotropic than the ring itself.

The linear stability analysis confirmed that ring Astrid is unstable to an $m = 2$ mode and that this is the fastest growing mode. Both the pattern and growth rate agree well with the developing perturbation during the first 10 days of time integration. Growth of the $m = 2$ mode eventually leads to ring splitting. In addition, a sensitivity study was performed by varying the strength of the ring, its radial profile, the barotropic component, and the diameter. Also the β-effect and the effect of cooling were investigated. All profiles we considered appear to be unstable to an $m = 2$ mode. For realistically strong rings the instability process leads in most cases to splitting of the ring, although in some cases the growth of the $m = 2$ mode equilibrated before splitting occurred. Equilibrated rings are characterized by a strong barotropic component in the parent ring. As a result, the barotropic energy conversion becomes dominant in the instability process and the $m = 2$ mode attains an almost purely barotropic character. In the nearly equilibrated SSH field the ring is accompanied by one, or more, almost barotropic cyclones. It is suggested that the stability of this equilibrated state of strong corotating rings and a barotropic $m = 2$ mode critically depends on the diameter of the ring.

For the decay of SSH the barotropic component appears to be essential. Only corotating rings with a strong barotropic component feature SSH decay; counterrotating rings may feature SSH increase. For counterrotating rings the parent ring features an energy conversion from the baroclinic to the barotropic component, while corotating rings show the reversed conversion. This suggests that growth of the $m = 2$ mode is associated with an interaction between the barotropic and baroclinic components within the parent ring, in such a way that the ring attains a nearly compensated structure. For corotating rings the decay of SSH critically depends on the stability of the ring related to the ring strength and the steepness of the radial velocity profile. More stable rings show less decay of SSH.

On the f-plane the instability process develops initially almost similar to that on the β-plane. Eventually, ring evolution on the β-plane becomes more asymmetric. It appears that in the nonlinear phase the β-effect plays a significant role on SSH decay. On the f-plane decay is much weaker. The conversion from available potential to kinetic energy is about a factor of two less. Also, the ring becomes less baroclinic. The impact of cooling on the decay of Agulhas rings is rather modest. Both the strong stratification and relatively weak air/sea

temperature contrasts seem to be responsible for this, by allowing little variation in the Rossby deformation radius.

For ring Astrid the decay of SSH scales well with the loss of passive tracer from the core of the ring. In the thermocline mixing of watermass characteristics preferably occurs through the lobes at the extremes of the elongated ring, modified by the developing $m = 2$ mode. In the deepest layer watermass exchange mainly occurs by dispersion through Rossby-wave radiation.

Acknowledgements

We thank Mathijs Schouten for producing Fig. 1. Hendrik van Aken and Astrid van Veldhoven are thanked for assisting in processing and analyzing the observational data from the MARE-cruises and producing Fig. 2a. Discussions with Will de Ruijter strongly stimulated and affected this work. The contribution of CAK was supported by the Foundation for Fundamental Research of Matter (FOM) under grant 00MV07, the contribution of LdS was supported by the Netherlands Organization for Scientific Research (NWO) under grant 750-712.00 B.

References

Beismann, J.-O., Käse, R.H., Lutjeharms, J.R.E., 1999. On the influence of submarine ridges on translation and stability of Agulhas rings. Journal of Geophysical Research 104, 7897–7906.

Benilov, E.S., Broutman, B., Kuznetsova, E.P., 1998. On the stability of large-amplitude vortices in a continuously stratified fluid on the f-plane. Journal of Fluid Mechanics 355, 139–162.

Bleck, R., Boudra, D.B., 1981. Initial testing of a numerical ocean circulation model using a hybrid (quasi-isopycnic) vertical coordinate. Journal of Physical Oceanography 11, 755–770.

Bleck, R., Smith, L.T., 1990. A wind-driven isopycnic coordinate model of the north and equatorial Atlantic ocean. 1. Model development and supporting experiments. Journal of Geophysical Research 95, 3273–3505.

Chassignet, E.P., Olson, D.B., Boudra, D.B., 1990. Motion and evolution of oceanic rings in a numerical model and in observations. Journal of Geophysical Research 95, 22121–22140.

De Ruijter, W.P.M., Biastoch, A., Drijfhout, S.S., Lutjeharms, J.R.E., Matano, R.P., Pichevin, T., Van Leeuwen, P.J., Weijer, W., 1999. Indian–Atlantic interocean exchange: dynamics, estimation and impact. Journal of Geophysical Research 104, 20885–20910.

Dewar, W.K., Killworth, P.D., 1995. On the stability of oceanic rings. Journal of Physical Oceanography 25, 1467–1487.

Dewar, W.K., Killworth, P.D., Blundell, J.R., 1999. Primitive-equation instability of wide ocean rings. Part II: numerical studies of ring stability. Journal of Physical Oceanography 29, 1744–1758.

Drijfhout, S.S., 1990. Eddy-genesis and the related transports of heat, momentum and vorticity: a parameter study. Journal of Physical Oceanography 20, 1645–1665.

Duncombe Rae, C.M., Garzoli, S.L., Gordon, A.L., 1996. The eddy field of the southeast Atlantic Ocean: a statistical census from the Benguela sources and transports project. Journal of Geophysical Research 101, 11949–11964.

Flierl, G.R., 1988. On the instability of geostrophic vortices. Journal of Fluid Mechanics 197, 349–388.

Garzoli, S.L., Gordon, A.L., Kamenkovich, V., Pillsbury, D., Duncombe Rae, C.M., 1996. Variability and sources of the southeastern Atlantic circulation. Journal of Marine Research 54, 1039–1071.

Goñi, G.J., Garzoli, S.L., Roubicek, A.J., Olson, D.B., Brown, O.B., 1997. Agulhas Ring dynamics from TOPEX/POSEIDON satellite altimeter data. Journal of Marine Research 55, 861–883.

Gordon, A.L., 1986. Interocean exchange of thermocline water. Journal of Geophysical Research 91, 5037–5046.

Gordon, A.L., Weiss, R.F., Smethie, W.M., Warner, M.J., 1992. Thermocline and intermediate water communication between the South Atlantic and Indian Oceans. Journal of Geophysical Research 97, 7223–7240.

Helfrich, K.R., Send, U., 1988. Finite-amplitude evolution of two-layer geostrophic vortices. Journal of Fluid Mechanics 197, 331–348.

Hogg, N.G., Stommel, H.M., 1985. Hetonic explosions: the breakup and spread of warm pools as explained by baroclinic point vortices. Journal of Atmospheric Sciences 42, 1465–1476.

Kamenkovich, V.M., Leonov, Y.P., Nechaev, D.A., Byrne, D.A., Gordon, A.L., 1996. On the influence of bottom topography on the Agulhas Eddy. Journal of Physical Oceanography 26, 892–912.

Killworth, P.D., Blundell, J.R., Dewar, W.K., 1997. Primitive-equation instability of wide oceanic rings. Part I: linear theory. Journal of Physical Oceanography 27, 941–962.

Kloosterziel, R.C., Van Heijst, G.J., 1989. On tripolar vortices. In: Nihoul, J.J., Jamart, B.M. (Eds.), Mesoscale/Synoptic Coherent Structures in Geophysical Turbulence. Elsevier, Amsterdam, pp. 609–625.

Lutjeharms, J.R.E., De Ruijter, W.P.M., Ridderinkhof, H., Van Aken, H., Veth, C., Van Leeuwen, P.J., Drijfhout, S.S., Jansen, J.H.F., Brummer, G.-J.A., 2000. MARE and ACSEX: new research programmes on the Agulhas Current system. South African Journal of Science 96, 105–110.

McDonald, N.R., 1998. The decay of cyclonic eddies by Rossby wave radiation. Journal of Fluid Mechanics 361, 237–252.

Nof, D., 1990. The role of angular momentum in the splitting of isolated eddies. Tellus 42, 469–481.

Peterson, R.G., Stramma, L., 1991. Upper-level circulation in the South Atlantic ocean. Progress in Oceanography 26, 1–73.

Ripa, P., 1989. On the stability of oceanic vortices. In: Nihoul, J.J., Jamart, B.M. (Eds.), Mesoscale/Synoptic Coherent Structures in Geophysical Turbulence. Elsevier, Amsterdam, pp. 167–179.

Saunders, P.M., 1973. The instability of a baroclinic vortex. Journal of Physical Oceanography 3, 61–65.

Schmitz, W.J., 1995. On the interbasin-scale thermohaline circulation. Review of Geophysics 33, 151–173.

Schouten, M.W., De Ruijter, W.P.M., Van Leeuwen, P.J., 2000. Translation, decay and splitting of Agulhas rings in the southeastern Atlantic Ocean. Journal of Geophysical Research 105, 21913–21925.

Van Aken, H.M., Van Veldhoven, A.K., Veth, C., De Ruijter, W.P.M., Van Leeuwen, P.J., Drijfhout, S.S., Whittle, C.P., Rouault, M., 2003. Observations of a young Agulhas ring, Astrid, during MARE, the Mixing of Agulhas Rings Experiment. Deep Sea Research, this issue (PII: S0967-0645(02)00383-1).

Van Ballegooyen, R.C., Gründlingh, M.L., Lutjeharms, J.R.E., 1994. Eddy fluxes of heat and salt from the southwest Indian Ocean into the southeast Atlantic Ocean: a case study. Journal of Geophysical Research 99, 14053–14070.